LBL-23359
Preprint

Lawrence Berkeley Laboratory
UNIVERSITY OF CALIFORNIA

RECEIVED
LAWRENCE
BERKELEY LABORATORY

AUG 21 1987

LIBRARY AND
DOCUMENTS SECTION

Submitted to Nuclear Physics A

PRE-EQUILIBRIUM NEUTRON EMISSION IN THE NUCLEON EXCHANGE TRANSPORT MODEL

J. Randrup and R. Vandenbosch

June 1987

TWO-WEEK LOAN COPY
This is a Library Circulating Copy,
which may be borrowed for two weeks

NUCLEAR SCIENCE DIVISION

Prepared for the U.S. Department of Energy under Contract DE-AC03-76SF00098

LBL-23359 c.2

DISCLAIMER

This document was prepared as an account of work sponsored by the United States Government. While this document is believed to contain correct information, neither the United States Government nor any agency thereof, nor the Regents of the University of California, nor any of their employees, makes any warranty, express or implied, or assumes any legal responsibility for the accuracy, completeness, or usefulness of any information, apparatus, product, or process disclosed, or represents that its use would not infringe privately owned rights. Reference herein to any specific commercial product, process, or service by its trade name, trademark, manufacturer, or otherwise, does not necessarily constitute or imply its endorsement, recommendation, or favoring by the United States Government or any agency thereof, or the Regents of the University of California. The views and opinions of authors expressed herein do not necessarily state or reflect those of the United States Government or any agency thereof or the Regents of the University of California.

LBL-23359

Pre-Equilibrium Neutron Emission in the Nucleon Exchange Transport Model*

Jørgen Randrup
Nuclear Science Division, Lawrence Berkeley Laboratory
University of California, Berkeley, California 94720

and

Robert Vandenbosch
Departments of Physics and Chemistry
University of Washington, Seattle, Washington 98195

June 23, 1987

Abstract:

We extend the Nucleon Exchange Transport model to include the emission of pre-equilibrium neutrons as a result of nucleon transfer to unbound states. The treatment takes account of the heating of the two nuclei caused by the energy dissipation and the cooling due to the pre-equilibrium emission. Furthermore, the transferred nucleons may induce cascading in the receptor nucleus by means of direct two-body scattering with the resident nucleons, based on a reduced, Pauli-blocked, energy-dependent free NN cross section. Qualitative agreement with experimental data is achieved, but the absolute multiplicities are systematically underestimated by about a factor of two. The dependence of multiplicity on bombarding energy is reproduced. The energy spectra and their variation with angle are generally reproduced, although the yield of the highest energy particles is sometimes underestimated.

* This work was supported in part by the Director, Office of High Energy and Nuclear Physics of the Department of Energy under contracts DE-AC03-76SF00098 and DE-AC06-81ER40048.

1 Introduction

The emission of fast, pre-equilibrium nucleons in heavy-ion induced reactions becomes an increasingly probable process as the bombarding speed is increased to values comparable to the speeds associated with the Fermi motion of the nucleons. Considerable progress in characterizing these particles has been achieved in recent years.[1]-[12] At a bombarding energy of 20 MeV/N, the probability for a pre-equilibrium neutron to be emitted in a typical reaction is near unity. The angular distributions are quite forward-peaked and the energy spectra are fairly hard, falling off rather slowly with increasing emission energy and extending to energies per nucleon several times that of the projectile. The multiplicity of pre-equilibrium particles seems to increase approximately linearly with the bombarding energy.[7] If one attempts to fit the angular dependence of the energy spectra in terms of a moving source parameterization, the apparent source has a velocity that is roughly half the beam velocity, which is several times the velocity of the composite system, and a "temperature" (slope parameter) that is several times larger than that of the equilibrated composite system.

The observation of appreciable yields of nucleons with velocities larger than the beam velocity has stimulated speculations about the mechanism at play. The possibility that the coupling between relative motion and Fermi motion could boost transferred particles sufficiently to produce such prompt emission was first noted by Bondorf in 1976.[13] The topic gained further momentum with the independently conceived work by Robel and Swiatecki,[14] who coined the term "Fermi jets" to characterize the mechanism. Concurrently, Bondorf *et al.* formulated a simple model for the phenomenon [15] and subsequently refined it considerably.[16] In this latter work the term "PEP's" (for promptly emitted particles) was introduced to cover both the pure Fermi jets (which, in the nomenclature of Swiatecki, are the nucleons that propagate undisturbed through the receptor nucleus before emission) and secondary prompt ejectiles resulting from cascading in the receptor. In the present work, the term "Fermi jets" is used fairly loosely and include all the promptly emitted nucleons caused by the nucleon transfer mechanism. A number of calculations based on this picture have since been reported.[17]-[20] Studies based on the Time-Dependent Hartree-Fock model have also been carried out.[21,22]

The present study is closely related to the study of Bondorf *et al.*[16] It is also similar in spirit to the recent work of Leray *et al.*[17] and differs from the alternative approach represented by the Boltzmann master equation.[24] The basic idea in Fermi jet model calculations is that, as the target and projectile make contact, some of the individual nucleons that are transferred may, under favorable kinematical conditions, be sufficiently energetic in the receptor nucleus to escape promptly, their energy boost arising from the coupling of the original internal (Fermi) velocity of the nucleon in the donor nucleus with the relative velocity of the reacting nuclei. Obviously, the resulting yield of such promptly emitted particles depends sensitively on the underlying dynamics of the nuclear collision, specifically its early stage when the relative velocity is largest.

There are several motivations for the present study. First, and foremost, it is desirable to employ a dynamical model that has been demonstrated to be capable of reproducing a large number of observables in reactions between complex nuclei. Therefore we have used the Nucleon Exchange Transport model,[25] which has no adjustable parameters and has successfully reproduced such diverse phenomena as energy dissipation in damped reactions,[26] entrance-channel mass asymmetry dependence of the probability for fusion,[27] and the time delay observed in collisions of very heavy nuclei as probed by electron-positron production.[28] With regard to dissipative reactions, the model successfully accounts for the energy loss dependencies of the variances of the N and Z distributions,[29] the magnitude and alignment of the transferred angular momentum,[30] and the partition of the excitation energy between projectile-like and target-like fragments.[31]

Second, we wish to determine to what extent one can understand the qualitative features of such pre-equilibrium emission, especially the apparent source velocity and the spectral shape, in terms of energy dissipation prior to the particular nucleon transfer that led to pre-equilibrium emission.

Third, it is of interest to investigate the importance of direct nucleon-nucleon collisions and explore the possibility that the jet mechanism may be be exploited to provide information, such as mean free paths, about nucleonic propagation through *excited* nuclear matter, an interesting general physical property that is not easily probed by other means.

2 Description of the Model

As mentioned above, the dynamical model underlying the present calculations is the so-called Nucleon Exchange Transport model, which has been described in the literature.[25] The reacting nuclei are considered as two Fermi-Dirac gases of individual nucleons moving within the two spherical one-body mean fields. The trajectory of the dinucleus is determined by the conservative Coulomb and nuclear (proximity) forces and the one-body dissipation resulting mainly from the exchange of nucleons.

The present calculations are carried out as follows. For a given value of the impact parameter, as specified by the initial orbital angular momentum L (equal to the conserved total angular momentum J), the dynamical evolution of the dinuclear system is determined by solving the nucleon exchange transport equations. A band of L-values of width ΔL corresponds to a cross section equal to $\Delta\sigma_L = \pi\hbar^2 L\Delta L/\mu E_{\rm rel}$, where μ is the reduced mass of the two nuclei and $E_{\rm rel} = \frac{1}{2}\mu V_{\rm rel}^2$ is their relative kinetic energy, *i.e.* the kinetic energy in the CM system. This provides the time-dependent configuration of the dinucleus, including the relative separation, $\mathbf{R} = (R, \theta)$, the (equivalent sharp) radii of the two reaction partners, R_A and R_B, their internal temperatures, τ_A and τ_B, and the effective radius of the neck through which the nucleons are transferred, $c_{\rm eff}$.

2.1 Inclusion of Fermi jets

The standard dynamical code is augmented by a routine that follows the fate of the individual transferred nucleons as they propagate through the receptor nucleus. For the purpose of the Fermi jet calculation, the reaction system is considered as two sharp uniform spherical potential wells. Their radii are $C_{A,B} = R_{A,B} - b^2/R_{A,B}$ (b=1 fm is the nuclear surface diffuseness) and their relative position is $\mathbf{R}$. The mean current of nucleons transferred from one nucleus to the other is given by $N_A = n_0 \pi c_{\rm eff}^2$ where $n_0 = \frac{1}{4}\rho\bar{v} \approx 0.263$ fm^{-2} 10^{22}s^{-1} is the standard one-way flux in nuclear matter and $\sigma_{\rm eff} = \pi c_{\rm eff}^2$ is the effective neck radius. The quantity N_A denotes the one-body transfer current, *i.e.* the mean number of nucleons attempting to transfer per unit time. If there were no blocking these would all succeed in transferring but when the Pauli exclusion principle is taken into account the actual rate of transfer is much reduced. In the present study, it is assumed that the mean currents from nucleus A to nucleus B are the same as those from B to A and, furthermore, that the neutron and proton currents are in proportion to the overall neutron and proton numbers of the combined system. Though rather rough, these approximations should be quite adequate for our present purpose, since they are expected to only affect the overall normalization by at most 10-20%. Therefore, on the basis of N_A, as provided by the dynamical model, it can be calculated how many neutrons $\Delta\nu_N$ and protons $\Delta\nu_Z$ attempt to transfer, on the average, during a given small time interval Δt. We use

$$\Delta\nu_N = N_N \Delta t \approx \frac{N}{A}\, n_0 \pi c_{\rm eff}^2 \ , \ \Delta\nu_Z = N_Z \Delta t \approx \frac{Z}{A}\, n_0 \pi c_{\rm eff}^2 \ , \tag{1}$$

where N and Z refer to the combined dinuclear system. [To ensure satisfactory numerical accuracy, the number of transfers actually considered for each time interval is enhanced by a suitable prescribed factor, usually $\sim 10^3$.]

The transfers are assumed to occur uniformly over a circular window of radius c_0 determined by the intersect of the two sharp spheres. Of course, a special prescription is required for positive surface separations, *i.e.* when $R > C_A + C_B$ and the geometrical neck radius c_0 vanishes. In this case, we have chosen to let the transferred nucleons originate at the two points where the dinuclear symmetry axis intersects the two spheres. The results are not very sensitive to the specific prescription adopted. [This feature is not obvious: although the transfer rate is fairly small for such distant configurations, the relative nuclear speed is largest at this time.]

The source of the transferred particles is an isotropic Fermi-Dirac gas having the instantaneous nuclear temperature. This assumption, that the excitation generated by previous transfers has already been fully equilibrated within each nucleus, corresponds to the idealization of a quick intrinsic relaxation time and is only expected to have approximate validity. When picking the velocity of a transferring nucleon the Fermi-Dirac distribution is properly weighted with the velocity component normal to the window (the standard "flux" factor). As a result of the relative translational motion of the two nuclei, and their individual overall rotations, the source in the donor nucleus has a certain "drift" velocity as seen from an observer residing in the receptor nucleus.

If the momentum of the transferred nucleon is denoted by $\mathbf{p}_1$, as seen in the receptor frame, the attempted transfer is realized with the probability that the momentum $\mathbf{p}_1$ is available in the receptor nucleus, $\bar{f}_1 = 1 - f(\mathbf{p}_1)$, where $f(\mathbf{p}_1)$ denotes the Fermi-Dirac occupation probability in the receptor gas. This condition guarantees that proper account is taken of the Pauli exclusion principle and thus ensures that the momentum distribution of the transferred nucleons is consistent with the distribution assumed in the derivation of the expressions for the transfer rates in the Nucleon Exchange Transport model. [When the blocking is considered, the momentum $\mathbf{p}_1$ should be referred to the local receptor frame, which is in motion relative to the overall receptor frame due to the nuclear rotation; after the transfer, the further fate of the nucleon is considered in the global receptor frame, which is comoving with the entire nucleus. The distinction between local and global frames is not very important in the present problem, since the nuclei have acquired only little rotation at the relatively early times when jetting occurs.]

If the transfer is accepted, the intruder nucleon is propagated through the receptor nucleus along its (straight) classical trajectory. During this propagation, it is assumed that the dinuclear configuration remains unaltered. This convenient simplification is justified when the nucleonic speed is large relative to the dinuclear velocities; it will introduce some distortion in the differential cross sections of the emitted particles. In general, the nucleon may suffer binary collisions with other nucleons residing in the receptor nucleus and in this manner it may change its velocity and give rise to cascading (see below). When a propagating nucleon reaches the equivalent sharp nuclear surface, it is checked whether the kinematics permits its ejection: it must be a neutron and its normal speed must suffice to overcome the depth of the nuclear potential well. [In the present study we only consider the possibility of neutron emission, since this is by far the most dominant process at the energies of interest. If these conditions are satisfied, the nucleon escapes with a probability equal to the quantal transmission coefficient over a diffuse potential step of height 45 MeV,[32]

$$T = 1 - \left(\frac{\sinh[\pi a(k_< - k_>)]}{\sinh[\pi a(k_< + k_>)]} \right)^2 , \tag{2}$$

Here $k_<$ and $k_>$ denote the wave numbers associated with the motion inside and outside the nucleus in the direction normal to the surface, and a nuclear diffuseness parameter $a = 0.5$ fm^{-1} is used. In a purely classical treatment, the transmission coefficient would be unity. However, as has been known from neutron absorption studies since the early days of nuclear physics, the quantal reflection from the potential step is quantitatively important close to the threshold.[33] The normal speed of an emitted nucleon is appropriately reduced, giving rise to a deflection of the trajectory, and the particle is subsequently transformed into the laboratory frame and "observed", *i.e.* collected in a suitable accumulative table, usually organized according to the energy and angle of the emitted particle.

Those agitated nucleons that do not succeed in escaping promptly are assumed to equilibrate with the residual nucleus and we do not consider the further fate of the ensuing hot fragment as it ultimately deexcites by sequential evaportion.

2.2 Inclusion of two-body collisions

As the intruder nucleon propagates through the receptor nucleus, it may experience direct two-body collisions with the resident nucleons. This effect is quantitatively significant and we incorporate it to all orders in the collision number. In a refined treatment, one need consider neutrons and protons separately. However, for the sake of simplicity, and in the spirit of the approximations discussed around eq. (1), we have based our calculations on the the isospin-averaged free NN scattering cross section [34]

$$\bar{\sigma}_{NN}^{\text{free}} = \frac{1}{2}\sigma_{pp} + \frac{1}{2}\sigma_{pn} \approx 34 + 620\ \mathrm{e}^{(E/27\ \mathrm{MeV})}\ \mathrm{mb}\ . \tag{3}$$

This approximation is expected to affect our results only at the level of a few percent.

In most of our calculations the free NN cross section, as given by the above expression, has been multiplied by one-half in order to obtain a mean free path at zero temperature more consistent with empirical observations.[35,36] This correction, which is attributed to the presence of the nuclear medium, is sometimes characterized in terms of an effective nucleon mass $m^\star \approx 0.5\ m$.[37] The resulting effective scattering cross section, $\sigma_{NN}^{\text{eff}} = 0.5\ \bar{\sigma}_{NN}^{\text{free}}$, determines the "classical" mean free path λ_0 of the propagating nucleon (*i.e.* the mean free path if there were no blocking) or, equivalently, the "classical" collision rate ν_0. This latter quantity is given by

$$\nu_0 =< \rho\sigma_{12}v_{12} >_2 = g \int \frac{\mathrm{d}\mathbf{p}_2}{h^3}\ f(\mathbf{p}_2)\ \sigma_{NN}^{\text{eff}}(E_{12})\ v_{12}\ . \tag{4}$$

Here $\rho \approx 0.17\ \mathrm{fm}^{-3}$ is the nucleon density and $g = 4$ is the spin-isospin degeneracy. Furthermore, $v_{12} = |\mathbf{v}_1 - \mathbf{v}_2|$ is the relative speed of the two colliding nucleons. The velocity of the intruder nucleon is denoted by $\mathbf{v}_1$ and we have $v_1 = \nu_0\lambda_0$. The velocity of the resident collision partner is $\mathbf{v}_2$ and $f(\mathbf{p}_2)$ is the corresponding Fermi-Dirac occupation probability. Since the scattering cross section depends on the *relative* energy E_{12}, the mean free path depends both on the energy of the intruder nucleon and on the temperature of the medium through which it propagates. The flux factor v_{12} will counteract, and to a large degree compensate, the strong increase of σ_{NN} at low energies (which is a technical advantage).

On the basis of the mean free path λ_0, a tentative path length is picked randomly and a tentative scattering angle is picked isotropically. The corresponding final momenta are $\mathbf{p}_1'$ and $\mathbf{p}_2'$. The Pauli blocking is taken into account by allowing such a tentative collision to occur only with the probability that the final state is available, $\bar{f}(\mathbf{p}_1')\bar{f}(\mathbf{p}_2')$. This condition reduces the actual collision rate from ν_0 to ν and, accordingly, increases the actual mean free path from λ_0 to λ, where

$$\nu =< \rho\sigma_{12}v_{12}\bar{f}_1'\bar{f}_2' >_2 = g \int \frac{\mathrm{d}\mathbf{p}_2}{h^3}\ f(\mathbf{p}_2)\ \sigma_{NN}^{\text{eff}}(E_{12})\ v_{12}\bar{f}(\mathbf{p}_1')\bar{f}(\mathbf{p}_2')\ . \tag{5}$$

It is often convenient to write $\lambda = \eta\lambda_0$, where $\eta = \nu_0/\nu$ is the so-called *blocking factor* which measures the relative increase in the mean free path effected by the Pauli exclusion. Its dependence on the energy of the intruder nucleon and the temperature of

the medium was first discussed in ref. [38], based on an isotropic energy-independent scattering cross section. Later on, more elaborate studies have been made.[35,39] Some typical values obtained for the mean free path are shown in fig. 1.

Whenever such a nucleon-nucleon collision occurs, the scattering partner is agitated and becomes an additional cascade nucleon which is also propagated. [It turns out to be sufficient to propagate only nucleons that are unbound; this is a substantial calculational advantage.] In this manner each transferred nucleon, and *all* generations of (unbound) cascading nucleons, are propagated through the nucleus until they arrive at the surface, where they may be emitted if the kinematics are favorable, as described earlier. It should be added that the heat loss due to the nucleon emission is incorporated self-consistently into the calculation of the dynamical reaction trajectory; the effect is typically only a few percent on the multiplicity.

This process is performed for each time interval Δt throughout the reaction. [In practice it suffices to consider only times up to when the relative velocity of the two nuclei has dropped to a value where pre-equilibrium emission is no longer significant.] The entire procedure can be repeated for different partial waves L contributing to a particular reaction.

3 Illustrative Results

In this section we show some examples of the time evolution of a reaction. We also show the effects of various ingredients of the model. Finally, we investigate dependencies on impact parameter and bombarding energy.

3.1 The Time Evolution of a Typical Collision

We show in fig. 2 the time dependence of a number of quantities for the $L = 46\hbar$ partial wave in a reaction of 402 MeV ^{20}Ne with ^{165}Ho. We have included the effect of two-body collisions in this illustration. It is seen that the pre-equilibrium emission rate reaches a maximum as the neck is opening up. The maximum in the rate occurs after there has been considerable kinetic energy damping and when the temperature of the projectile-like fragment has nearly reached its maximum value. The fact that considerable kinetic energy damping has occurred before the most probable time for pre-equilibrium emission may account for the fact that the apparent source velocity derived from fits to data is only about half of the beam velocity. The fact that there has been appreciable heating due to energy dissipation is important in generating the most energetic particles.

Pre-equilibrium neutrons originating in the projectile are generally forward-peaked, and those from the target backward-peaked. The separation between the two components depends on the bombarding energy and the impact parameter. An example of the angular distributions of the two components integrated over $L = 0$ to $62\hbar$, is shown in fig. 3.

3.2 Influence of Various Ingredients in the Model

The simplest version of the model we have considered is one where the heating of the nuclei during the collision is neglected, and where the scattering of the transferred particles due to two-body collisions is also ignored. This gives rise to a relatively soft and very forward-peaked angular distribution. Including the effect of selecting nucleons from the appropriately heated gas leads to a large increase in the yield of the most energetic particles, as can be seen in fig. 4. Finally, inclusion of two-body scattering increases the yield at intermediate and backward angles. It also makes the energy spectra more exponential at forward angles, and, perhaps surprisingly, increases the apparent temperature characterizing the slope of the spectra.

The dependence of the multiplicity of pre-equilibrium neutrons on these ingredients is shown in fig. 5. It is seen that including the heating effect leads to an increased multiplicity, because a larger fraction of the transferred particles have sufficient kinetic energy to escape from the receptor nucleus. The decrease in the yield with inclusion of nucleon-nucleon scattering is due to the fact that the more energetic particles, which have a higher chance of escaping, are more likely to lose than gain energy in a collision. As mentioned previously, we have used an effective nucleon-nucleon scattering cross section to account for medium effects on the mean free path. In a test calculation for ^{20}Ne + ^{165}Ho at 402 MeV, we find that doubling the cross section, *i.e.* halving the mean free path, results in an additional reduction of 46% in the multiplicity of neutrons originating in the projectile-like particle. The effect on neutrons originating in the target-like partner is only 12%, since the dimensions of the receptor nucleus, ^{20}Ne, is comparable to the mean free path.

3.3 Dependence of Multiplicity on Bombarding Energy, Impact Parameter, and Entrance-Channel Mass Asymmetry

It can be seen from fig. 5 that the multiplicity increases linearly with bombarding energy for the ^{20}Ne + ^{165}Ho system. Furthermore, we find that for a particular partial wave, for this mass-asymmetric entrance channel, the multiplicity increases approximately in proportion to the energy above the Coulomb barrier, rather than as the speed at the point of contact. This result is consistent with the trend shown by Holub *et al.*[7] who compiled the results of a number of studies of asymmetric systems, although the scatter in the data precludes a quantitative conclusion.

This is not a general result for all systems, however. We have also performed calculations for the symmetric entrance channel leading to the same compound nucleus, and find a faster-than-linear increase of the multiplicity with bombarding energy. We have also tested the scaling used in some attempts to systematize the missing momentum transfer in incomplete fusion reactions (ref. [40]). We show in Fig. 6 the multiplicities calculated for the two entrance channels as a function of the velocity at contact. Neither system exhibits a scaling according to the velocity, and the more symmetric system exhibits a higher multiplicity for a given velocity. We attribute this latter result to both the larger window which develops in the more symmetric system

and the fact that for transfers originating in the projectile the smaller receptor nucleus in the symmetric system gives rise to less attenuation by two-body scattering. It is interesting to note that a recent study (ref. [41]) of the more symmetric reaction ^{40}Ar + ^{68}Zn has shown a larger missing momentum at a given net relative velocity than given by the systematics for the more asymmetric systems.

It should be remembered that a direct comparison between neutron jet multiplicity and missing momentum is not valid. As the bombarding energy increases pre-equilibrium α emission becomes increasingly important and is known to account for a sizeable fraction of the missing momentum.

The dependence of the multiplicity on impact parameter at 402 MeV is shown in fig. 7. The multiplicity is fairly constant over the L-range leading to evaporation residues in a sharp-cutoff approximation (0-69$\hbar$),[7] but is falling fairly rapidly over the L-range corresponding to fission (70-105$\hbar$). This latter result is in contrast to that reported by Leray *et al.*, where the multiplicity remains larger than half its maximum value through L=110$\hbar$. We attribute the falloff observed in our calculations to the decrease in the radial kinetic energy at contact as L increases.

4 Comparison with Experiment

In this section we compare the results of our calculations with measured total multiplicities and energy spectra at various angles. We consider first the results of Holub *et al.*[7] and Hilscher *et al.*,[12] which provides an extensive body of data for the ^{20}Ne + ^{165}Ho system covering the bombarding energy range from 11 to 30 MeV/N. Results are presented separately for multiplicities in coincidence with evaporation residues and in coincidence with fission fragments. We concentrate our attention on the former, where there is less sensitivity to the dependencies on the range of L-values contributing to the class of events under consideration.

We show first in fig. 8 the comparison of the bombarding energy dependence of the pre-equilibrium multiplicities. The experimental data are based on a decomposition of the energy spectra at different angles into evaporation and pre-equilibrium components each with a single source velocity. Two curves are shown: the lower curve is the pre-equilibrium multiplicity for neutrons originating in the projectile, and the upper (dashed) curve includes also neutrons originating in the target. Since the latter have lower energy and are less forward peaked they are likely to be at least partially included in the evaporative component in the decomposition of the experimental spectrum. Thus it is probably most appropriate to compare the data with the lower curve. This comparison suggests that the present calculations somewhat underestimate the yields. We emphasize at this point that no parameters have been adjusted to attempt to fit experimental multiplicity data.

We turn now to an examination of the energy spectra at various angles. Comparison with the results of Holub *et al.*[7] at 402 MeV are shown in fig. 9. The calculations give about the correct yield at the intermediate energies and most forward angles, where most of the neutrons are emitted. It fails, however, to account for the highest-

energy neutrons. This is in contrast to the model of Leray *et al.*, whose calculated spectra are harder in spite of the fact that their nucleons are picked from a cold Fermi gas. Leray *et al.* account for the loss of primary particles by means of an absorptive imaginary potential but otherwise neglect two-body scattering, which we find to be important because the mean free path even in cold nuclear matter is only about half the diameter of the target nucleus. We have also compared our model with the energy spectra of neutrons in coincidence with fission fragments reported by Kasagi *et al.* [11] for the $^{16}O + ^{238}U$ reaction at 20 MeV/N. These data are in coincidence with a single fission fragment detected near 90°. The inclusive fission cross section is not known at this energy. We have performed calculations for an L range between 0 and $100\hbar$. [Another calculation extending up to $L = 140\hbar$ gives very similar spectra as the neutron multiplicity is falling off rapidly for L values above $100\hbar$.] With this range our calculated absolute multiplicities are again a factor of about two too low, but the shapes of the energy spectra are remarkably well reproduced, as is the angular distribution. This is illustrated in fig. 10 where we show the results of our calculations multiplied by a factor of two. The overall comparison with the data of Holub *et al.* in fig. 9 would also be improved if the calculated spectra were multiplied by a factor of two.

We have examined the stability of our results with respect to certain assumptions. We have tested an alternate form of the medium correction to the free nucleon-nucleon cross sections by evaluating the expression for $\bar{\sigma}_{NN}^{\text{free}}(E)$ in eq. (3) at an effective energy of twice the actual energy, rather than simply multiplying the free cross section by one half. Such a change reduces the differential cross section somewhat at forward angles and hardens the spectrum at 90° for 402 MeV $^{20}Ne + ^{165}Ho$. The multiplicity of neutrons induced by transfer from the projectile dropped by about 15%. Thus some of our results are sensitive to details of the two-body scattering but the total multiplicity is less so.

We have also considered the possibility that our jet particle angular distributions are too sharply peaked due to the classical way the particle is propagated through and out of the receptor. Mantzouranis *et al.*[42] have pointed out that there is a quantum mechanical indeterminacy in angle dependent on the maximum angular momentum the emitted particle can have. They evaluate the full width of this delocalization to be $\theta_m = 2\pi/k_\perp R = \mathrm{h}/l$, where $l = \hbar k_\perp R$ is the angular momentum of the nucleon. We have performed an approximate test of this effect by introducing a dispersion of this magnitude on to the emission direction of the particle as it leaves the receptor nucleus. The effect of this spreading is discernible in an energy-projected angular distribution but is not apparent in a plot such as given in fig. 9. The relative insignificance of this refinement probably arises from the fact that considerable angular dispersion is already introduced by the random nature of the original Fermi motion and by two-body scattering. Much of the final sharpness of the observed angular distribution arises from the transformation to the laboratory system. This is particularly true for the lower-energy particles for which the quantum mechanical spread is largest.

Finally, we have investigated the effect of assuming that the nucleon mass is re-

duced to $m_{\rm eff} = 0.5\ m_{\rm free}$ inside the nuclear medium. Since the Fermi momentum remains unaltered (the nucleon density $\rho \sim P_F^3$ stays the same), the constituent nucleons acquire speeds that are typically twice as large. Furthermore, in order to retain the same chemical potential $\mu \approx -8$ MeV, the potential is correspondingly deeper: rather than the ordinary value of ≈45 MeV it should now be ≈82 MeV. Because the nucleonic velocity is doubled, so is the kinetic energy increase arising from the boost by the relative nuclear motion. (However, because of the lighter mass and the higher potential step, the energy of an emitted nucleon is only affected rather little.) It is not obvious what the appropriate scattering cross section should be. We have used the free scattering cross section (3), without the reduction by one half, but evaluated at the increased (≈doubled) kinetic energy. This results in a generally substantially increased mean free path of the propagating nucleons. At the surface there is energy conservation (the nucleon motion is still governed by a time-independent Hamiltonian, even though the mass is now position dependent) and conservation of the angular momentum (the Hamiltonian is rotationally invariant). The net result is a reduction of the jet multiplicity by typically 30% at the highest bombarding energy, probably because there is much less cascading. Furthermore, the most probable ejection energy is shifted upwards somewhat, whereas the spectral fall-off is faster. In view of the theoretical uncertainties associated with the consistent incorportion of off-shell effects, we have not, for the results presented in this paper, attempted to further refine the treatment but have employed the simple halving of the scattering cross section throughout.

We turn now to a comparison of our model with the results of a rather different kind of experiment. Remington *et al.*[10] have examined the neutron energy spectra on both sides of the beam when a projectile-like fragment is detected on a particular side of the beam. They present neutron spectra gated by different Z-values and by specific kinetic energy ranges of the detected projectile-like fragment. We concentrate on events where a Z=6 (carbon) fragment is detected in ^{14}N bombardment of ^{165}Ho. Events with lower Z-values likely result with increasing probability from sequential decay of projectile-like fragments. In our particular example, the neutron spectra were gated by carbon ions with laboratory kinetic energies between 300 and 470 MeV. Comparison with the predictions of the transport model suggest that partial waves between $L = 115\hbar$ and $L = 165\hbar$ contribute to these inelasticities, and that scattering to a negative deflection angle has accurred for most of the contributing partial waves, *i.e.* a projectile initially approaching with a "positive" impact parameter is pulled through the beam direction so that it emerges with a "negative" deflection angle. It is interesting to note that Tsang[43] has reported negative deflection angles for carbon fragments in this reaction, although her observationwas made at 35° whereas we compare with Remington's results [10] obtained with the carbon detector at 10°. We compare our results for the neutron energy spectra at positive and negative angles (*i.e.* for neutrons emerging on the same and opposite sides of the beam as the projectile-like fragment) with the results of Remington.[10] There is one overall normalization involved, as we are not in a position to quantitatively predict the fractionation of the different L-values between different possible combinations of Z and energy loss

of the projectile-like fragments. It is seen from fig. 11 that the calculations account for most of the characteristic features observed. The slopes of the energy spectra are generally in agreement with experiment except for the smallest angle, where an additional contribution from sequential neutron decay of a projectile-like fragment (*e.g.*, ^{13}C) is expected. The near-equality of yields on both sides of the beam for the most forward and backward angles is also reproduced, as is the enhancement of neutrons on the opposite side of the beam at intermediate angles. The latter arise in our calculations from neutrons induced by transfers from the target to the projectile.

5 Concluding Remarks

We have presented an extension of the Nucleon Exchange Transport model, incorporating the effects of nucleon transfer to unbound states which may lead to promptly emitted neutrons. We demonstrate the importance of including the heating of the reaction partners due to previous exchanges (and the dissipation associated with the neck evolution). An examination of the time dependence of the collision reveals that the temperature of the projectile-like fragment is near its maximum value when the jet production is at its maximum. We have also demonstrated the importance of two-body scattering in the receptor nucleus. Careful attention has been paid to the energy dependence of the scattering and to Pauli blocking. Two-body scattering attenuates the multiplicity of pre-equilibrium neutrons, softens the shape of their energy spectra, and broadens their angular distribution.

We have compared the model with two classes of experimental data, one emphasizing the more central collisions, and another involving more peripheral reactions. No adjustments of parameters to fit data have been made. The bombarding energy dependence of the jet multiplicity for the more central collisions (fusion leading to evaporation residues) is well reproduced, although the absolute multiplicity is somewhat underestimated. The latter difficulty might be relieved by the use of a longer mean free path, as our choice of the effective nucleon-nucleon cross section leads to mean free paths close to the lower limits of empirical determinations. The high-energy tails of the neutron spectra reported by Holub *et al.*[7] for fusion reactions are somewhat underestimated by our model, although we reproduce the spectra of Kasagi *et al.*[12] and of Remington *et al.*[10] quite well. For the latter results we also reproduce quite well the angular distributions and a preponderance of neutrons at intermediate angles on the side of the beam corresponding to transfer from the target to the projectile. Possible refinements of the model have also been explored.

After the completion of this work we have, through a private communication, become aware of a similar study by S. Bhattarcharyya *et al.*.[44] The results of the two studies seem to be in general agreement.

We thank J.J. Griffin for a helpful comment on mean free paths, and D. Hilscher and B. Remington for providing us with data prior to publication. This work was supported in part by the Director, Office of High Energy and Nuclear Physics of the Department of Energy under contracts DE-AC03-76SF00098 and DE-AC06-81ER40048.

References

[1] L. Westerberg, D.G. Sarantites, D.C. Hensley, R.A. Dayras, M.L. Halbert, and J.H. Barker, Phys. Rev. **C18** (1978) 796.

[2] A. Gavron, J.R. Beene, R.L. Ferguson, F.E. Obenshain, F. Plasil, G.R. Young, G.A. Pettitt, K. Geoffroy Young, M. Jääskeläinen, D.G. Sarantities, and C.F. Maguire, Phys. Rev. **C24** (1981) 2048.

[3] A. Gavron, J.R. Beene, B. Cheynis, R.L. Ferguson, F.E. Obenshain, F. Plasil, G.R. Young, G.A. Petitt, C.F. Maguire, D.G. Sarantites, M. Jääskeläinen, and K. Geoffroy-Young, Phys. Rev. **C27** (1983) 450.

[4] A. Gavron, J.R. Beene, B. Cheynis, R.L. Ferguson, F.E. Obenshain, F. Plasil, G.R. Young, G.A. Pettit, M. Jääskeläinen, D.G. Sarantites, and C.F. Maguire, Phys. Rev. Lett. **47** (1981) 1255; **48** (1982) 835(E).

[5] T.C. Awes, G. Poggi, C.K. Gelbke, B.B. Back, B.G. Glagola, H. Breuer, and V.E. Viola, Phys. Rev. **C24** (1981) 89.

[6] K. Geoffroy-Young, D.G. Sarantites, J.R. Beene, M.L. Halbert, D.C. Hensley, R.A. Dayras, and J.H. Barker, Phys. Rev. **C23** (1981) 2479.

[7] E. Holub, D. Hilscher, G. Ingold, U. Jahnke, H. Orf, and R. Rossner, Phys. Rev. **C28** (1983) 252.

[8] E. Holub, D. Hilscher, G. Ingold, U. Jahnke, H. Orf, H. Rossner, W.P. Zank, W.U. Schröder, H. Gemmeke, K. Keller, L. Lassen, and W. Lücking, Phys. Rev. **C33** (1986) 143.

[9] J.L. Laville, C. LeBrun, J.F. Lecolley, F. Lefebres, M. Louvel, R. Regimbart, J.C. Steckmeyer, R. Bertholet, C. Guet, D. Heuer, M. Maurel, H. Nifenecker, C. Ristori, F. Schlusser, F. Guilbault, and C. Lebrun, Phys. Lett. **156B** (1985) 42.

[10] B.A. Remington, G. Caskey, A. Galonsky, C.K. Gelbke, L. Heilbrown, J. Heltsley, M.B. Tsang, F. Deak, A. Kiss, Z. Seres, J. Kasagi, and J.J. Kolata, Phys. Rev. **C34** (1986) 1689, and private communication.

[11] J. Kasagi, S. Saini, T.C. Awes, A. Galonsky, C.K. Gelbke, G. Poggi, D.K. Scott, K.L. Wolf, and R.L. Legrain Phys. Lett. **104B** (1981) 434.

[12] D. Hilscher, H. Rossner, A. Gamp, U. Jahnke, B. Cheynis, B. Chambon, D. Drain, C. Pastor, A. Giorni, C. Morand, A. Dauchy, P. Stassi, and G.A. Petitt, Phys. Rev. **C** (in press).

[13] J.P. Bondorf, J. de Phys. **C5** (1976) 195.

[14] M.C. Robel, Ph.D. Thesis, LBL-8181 (1979) unpublished.

[15] J.P. Bondorf, J.N. De, A.O.T. Karvinen, G. Fai, and B. Jakobsson, Phys. Lett. **84B** (1979) 162.

[16] J.P. Bondorf, J.N. De, G. Fai, A.O.T. Karvinen, B. Jakobsson, and J. Randrup, Nucl. Phys. **A333** (1980) 285.

[17] S. Leray, G. La Rana, C. Ngo, M. Barranco, M. Pi, and X. Vinas, Z. Phys. **A320** (1985) 383.

[18] K. Möhring, W.J. Swiatecki, and Z. Zrelinska-Pfabe, Nucl. Phys. **A440** (1985) 89.

[19] F. Sebille and B. Remaud, Nucl. Phys. A 420 (1984) 141.

[20] H.S. Köhler, Nucl. Phys. **A438** (1985) 564.

[21] K.R.S. Devi, M.R. Strayer, K.T.R. Davies, S.E. Koonin, and A.K. Dhar, Phys. Rev. **C24** (1981) 2521.

[22] S.H. Köhler, Acta Phys. Pol. **B13** (1982) 107.

[23] A.S. Umar, M.R. Strayer, D.J. Ernst, and K.R. Sandhya Devi, Phys. Rev. **C30** (1984) 1934.

[24] M. Blann, Phys. Rev. **C23** (1981) 205; M. Blann, Phys. Rev. **C31** (1985) 1245; M. Blann, Phys. Rev. **C35** (1987) 1581.

[25] J. Randrup, Nucl. Phys. **A327** (1979) 490; Nucl. Phys. **A383** (1983) 468; T. Døssing and J. Randrup, Nucl. Phys. **A433** (1985) 215.

[26] W.U. Schröder and J.R. Huizenga, in "Treatise on Heavy-Ion Science," D. Allan Bromley, ed., Plenum, 1984, Vol. 2, p. 115.

[27] R. Vandenbosch, in "Heavy Ion Fusion Reactions," K. Furuno and T. Kishimoto, eds., World Scientific, 1985, p. 355.

[28] R. Krieg, E. Bożek, U. Gollerthan, E. Kankeleit, G. Klotz-Engmann, M. Krämer, U. Meyer, H. Oeschler, and P. Senger, Phys. Rev. **C34** (1986) 562.

[29] W.U. Schröder, J.R. Huizenga, and J. Randrup, Phys. Lett. **98B** (1981) 355; H.C. Britt, B.K. Erkkila, A. Gavron, Y. Patin, R.H. Stokes, M.P. Webb, P.R. Christensen, O. Hansen, S. Pontoppidan, F. Videbaek, R.L. Ferguson, F. Plasil, G.R. Young, and J. Randrup, Phys. Rev. **C26** (1982) 1999; D.-K. Lock, R. Vandenbosch, and J. Randrup, Phys. Rev. **C31** (1985) 1268.

[30] T. Døssing and J. Randrup, Nucl. Phys. **A433** (1985) 280.

[31] R. Vandenbosch, A. Lazzarini, D. Leach, D.-K. Lock, A. Ray, and A. Seamster, Phys. Rev. Lett. **52** (1984) 1964.

[32] L.D. Landau and E.M. Lifshitz, "Quantum Mechanics, Non Relativistic Theory," translated from Russian by J.B. Sykes and J.S. Bell, Pergamon Press 1958, p. 76.

[33] B.R. Mottelson, Niels Bohr Centennial Conference on Nuclear Structure 1985, Copenhagen, May 20-24, 1985, North Holland, Eds. R.A. Broglia *et al.*, p. 3.

[34] K. Chen, Z. Fraenkel, G. Friedlander, J.R. Grover, J.M. Miller, and Y. Shimamoto, Phys. Rev. **166** (1968) 949.

[35] M.T. Collins and J.J. Griffin, Nucl. Phys. **A348** (1980) 63.

[36] A. Nadasen, P. Schwandt, P.P. Singh, W.W. Jacobs, A.D. Bacher, P.T. Debevec, M.D. Kailchuck, and J.T. Meek, Phys. Rev. **C23** (1981) 1023.

[37] J.W. Negele and K. Yazaki, Phys. Rev. Lett. **47** (1981) 71; S. Fantoni, B.L. Friman, and V.R. Panharipande, Phys. Lett. **B104** (1981) 89.

[38] J. Randrup, Proceedings of the Symposium on Heavy Ion Physics from 10 to 200 MeV/AMU, Brookhaven National Laboratory, July 16-20, 1979, p. 713.

[39] B. Sinha, Phys. Rev. Lett. **50** (1983) 91.

[40] V.E. Viola, Jr., B.B. Back, K.L. Wolf, T.C. Awes, C.K. Gelbke and H. Breuer, Phys.Rev. **C26** (1982) 178.

[41] A. Fahli, J.P. Coffin, G. Guillame, B. Heusch, F. Jundt, F. Rami, P. Wagner, P. Fintz, A.J. Cole, S. Kox, and Y. Schultz, submitted to Phys. Rev. **C**.

[42] G. Mantzouranis, H.A. Weidenmüller, and D. Agassi, Z. Physik **A276** (1976) 145.

[43] M.B. Tsang, Proceedings of the ACS Symposium on Central Collisions and Fragmentation Processes, Denver, Colorado, April 5-10, 1987, North Holland, C.K. Gelbke, ed., (in press).

[44] S. Bhattarcharyya, K. Krishan, S.K. Samaddar, and J.N. De, private communication (1987).

Figure captions

Figure 1

The mean free path λ employed in the calculation, shown as a function of the temperature of the medium, τ, for three values of the (asymptotic) energy of the intruder nucleon, E_0, as calculated by using half the free NN scattering cross section given in eq. (3), $\sigma_{NN}^{\text{eff}} = 0.5\ \bar{\sigma}_{NN}^{\text{eff}}$.

Figure 2

The time evolution of a typical collision. The upper panel (a) shows the radial component of the kinetic energy. The second panel (b) shows the internuclear separation R (upper curve) and the neck radius; the solid curve is the radius of the cylindrical neck c_0 and the dashed curve is the effective neck radius c_{eff} which includes the effect of the juxtaposed diffuse surfaces outside the cylinder. The third panel (c) shows the temperature of the projectile-like nuclide, τ_A (solid curve), and that of the target-like nuclide, τ_B (dashed curve). The fourth panel (e) shows the time-differential multiplicity of emitted neutrons induced by transfer from the projectile, *i.e.* the time-dependent total neutron emission rate.

Figure 3

The angular distribution of preequilibrium neutrons induced by transfer from the projectile (solid curve) and the target (dashed curve).

Figure 4

Illustration of various ingredients of the model on the energy spectra at different angles. The dashed curves neglect temperature and two-body collisions, the long-dashed curve includes the time-dependent temperatures τ_A and τ_B, and the solid curve includes both the temperature and the two-body collisions.

Figure 5

Dependence of the multiplicity of pre-equilibrium neutrons induced by transfer from the projectile without temperature or two-body scattering (dashed curve), with temperature (long dashed curve), and with both temperature and two-body scattering (solid curve).

Figure 6
Comparison of multiplicity of pre-equilibrium neutrons produced by transfers from the projectile nucleus, for two entrance channels of different mass asymmetry leading to the same compound nucleus, plotted as a function of the relative speed at contact, $V_{\text{contact}} = \sqrt{2(E_{CM} - V_C)/\mu}$.

Figure 7
Dependence of the multiplicity of pre-equilibrium neutrons on the initial angular momentum L. The full and dashed curves are the multiplicities for neutrons originating in the projectile and target, respectively.

Figure 8
Comparison of the calculated multiplicity of pre-equilibrium neutrons with the measured multiplicities of Holub *et al.* [7] and Hilscher *et al.* [12], as a function of the bombarding energy. The experimental multiplicities are based on a moving source fit and hence represent to lowest order only the multiplicity of neutrons originating in the projectile. The full and dashed curves are the multiplicities for neutrons induced by transfer from the projectile or target, respectively.

Figure 9
Comparison of the calculated energy spectra (solid curves) at different angles with the measurements of Holub *et al.* [7] (dots). The dashed curves at low energies represent their fit to the evaporation component.

Figure 10
Comparison of calculated energy spectra at different angles (solid curves) with the data of Kasagi *et al.*.[11] The calculated results have been multiplied by an overall factor of two to exhibit the agreement with the measured slopes and angular variation. The dashed curves are the fitted evaporative contributions.

Figure 11
Comparison of neutron spectra at various angles and on different sides of the beam, relative to the side where the projectile-like fragment is predicted or observed. The experimental data [10] are gated on Z=6 fragments detected at 10°. The calculated results are indicated by dashed and solid curves for emission on the same or the opposite side as the projectile-like fragment, respectively.

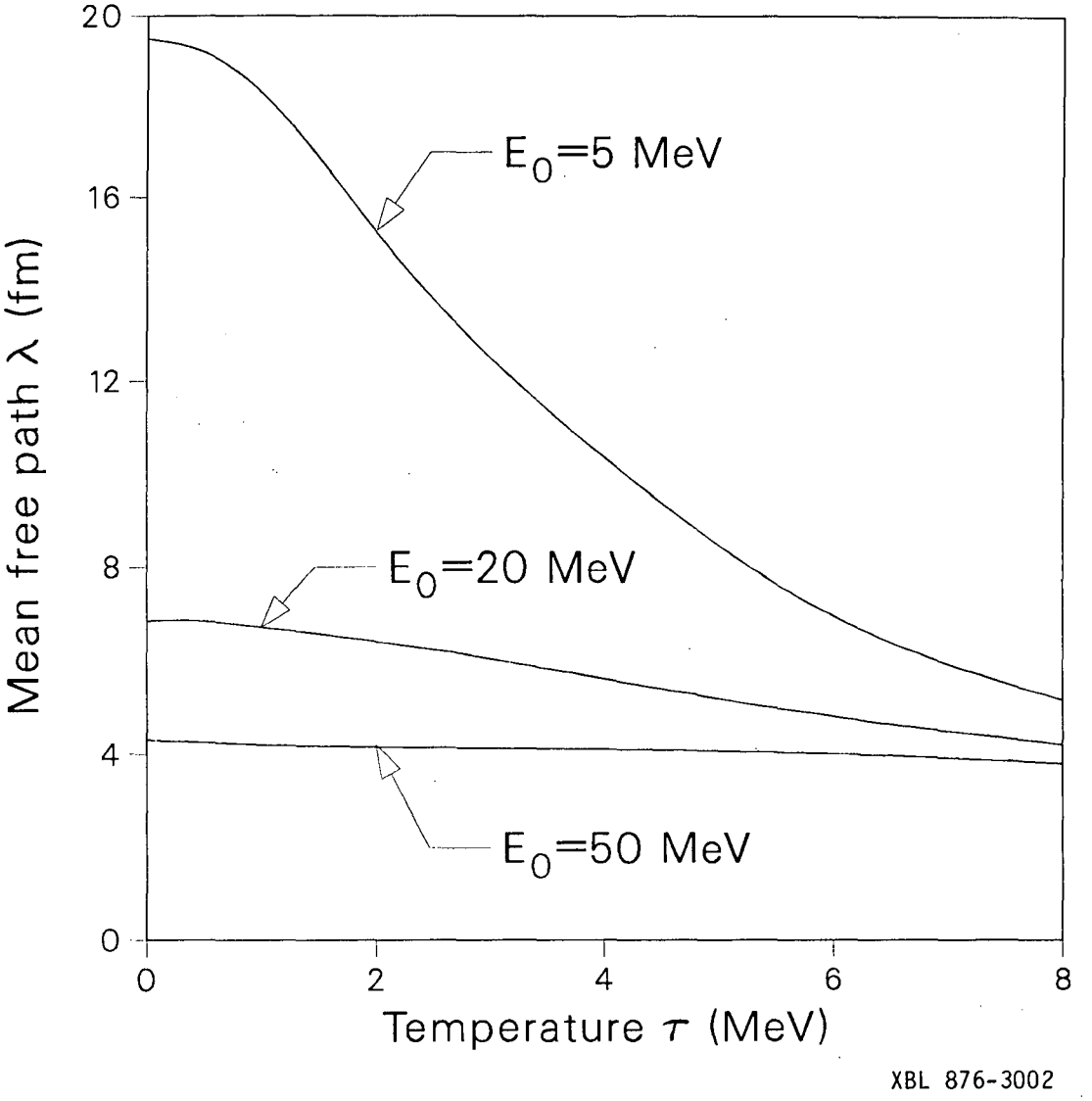
20
16
12
8
4
0
Mean free path λ (fm)
E0=5 MeV
E0=20 MeV
E0=50 MeV
0
2
4
6
8
Temperature τ (MeV)
XBL 876-3002

Figure 1.

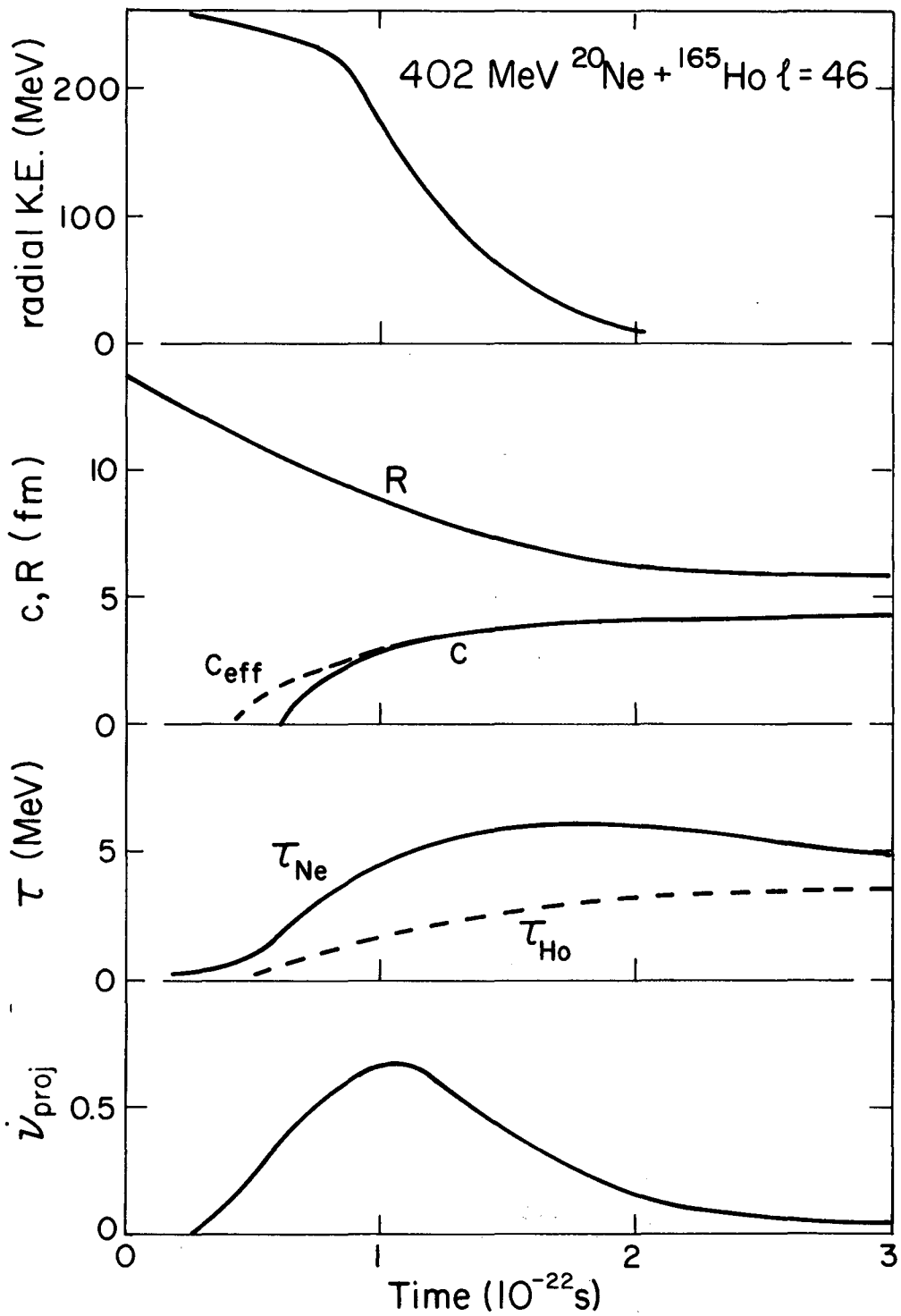

XBL 876-3003

Figure 2.

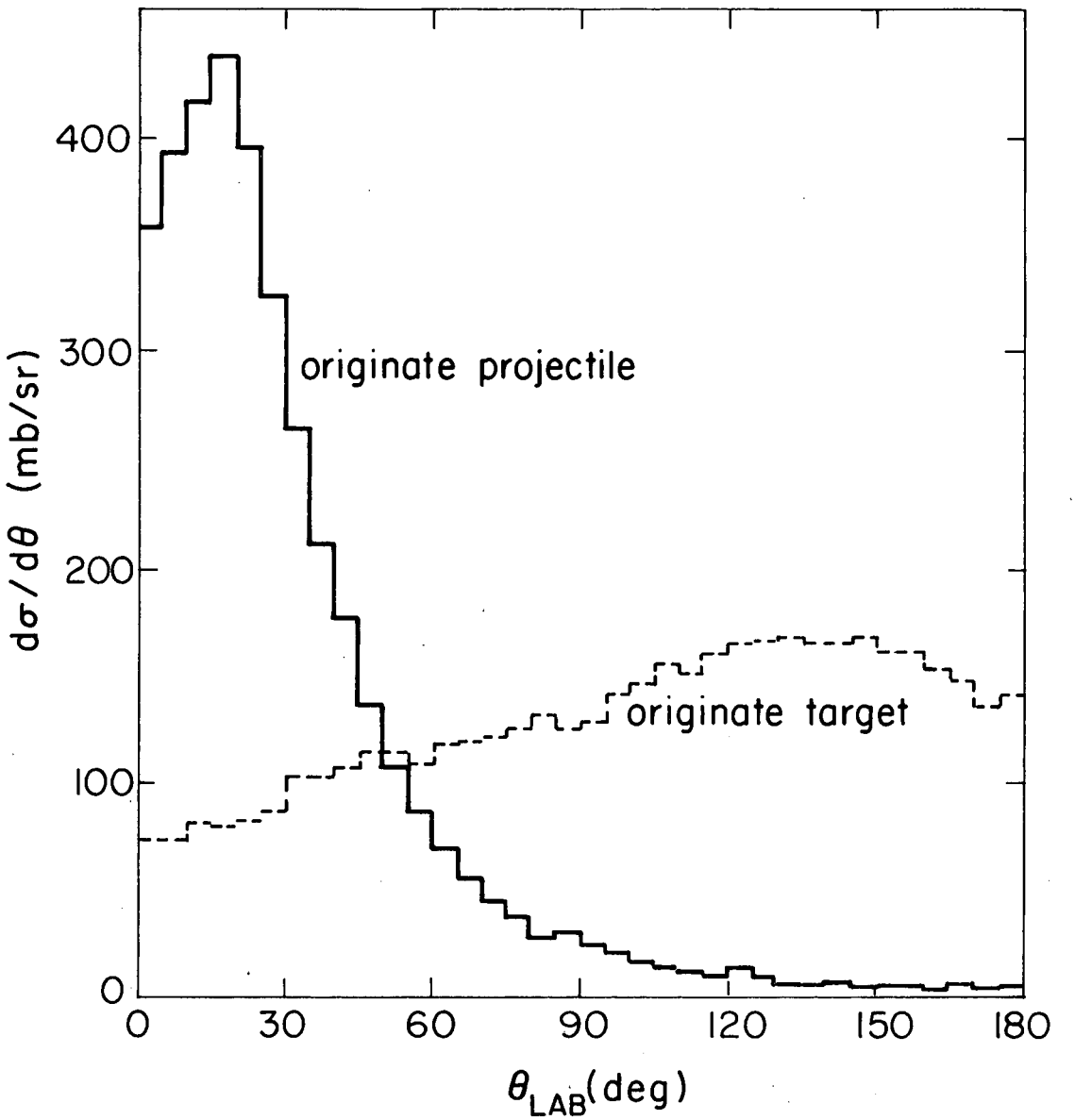

XBL 876-3004

Figure 3.

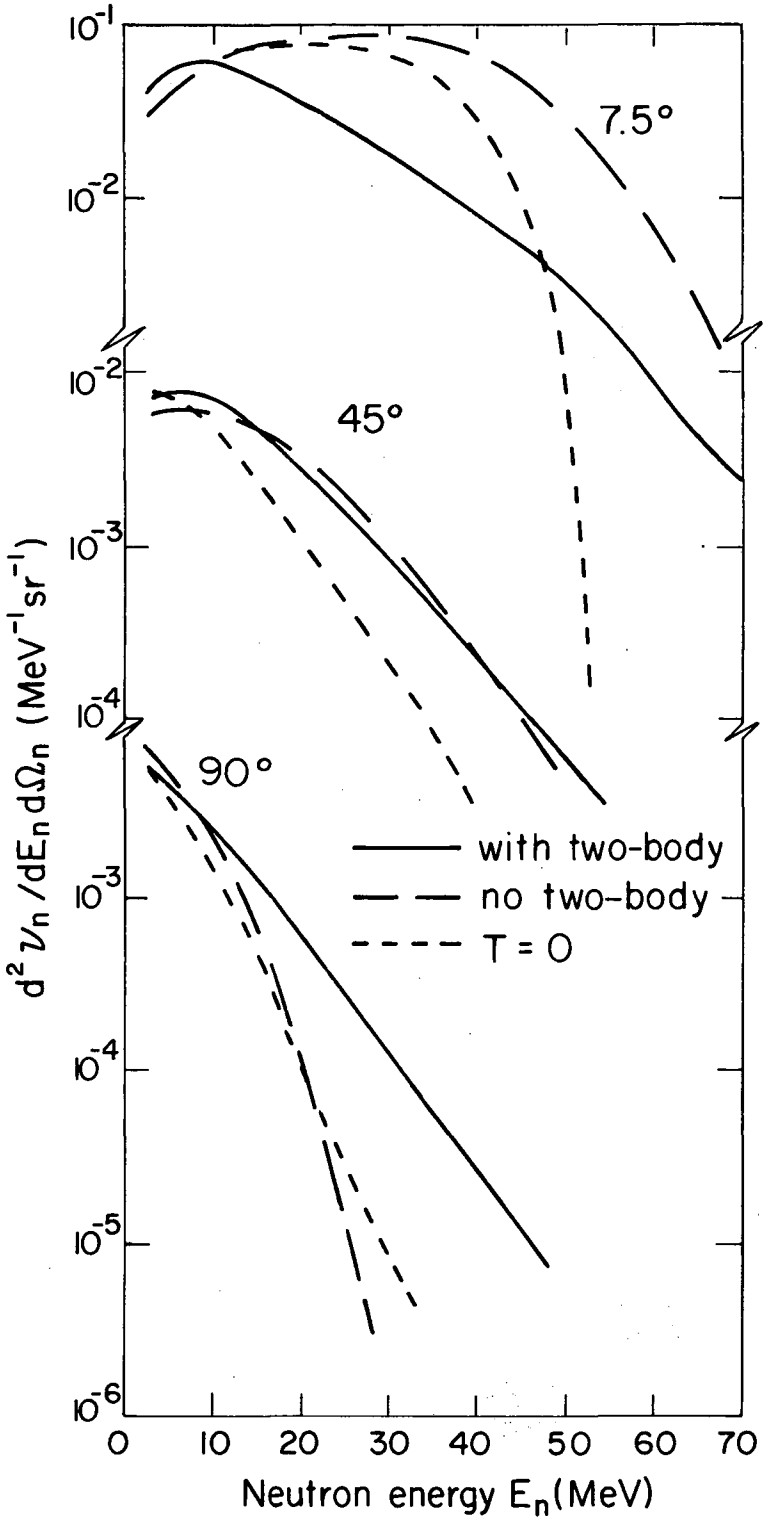

XBL 876-3005

Figure 4.

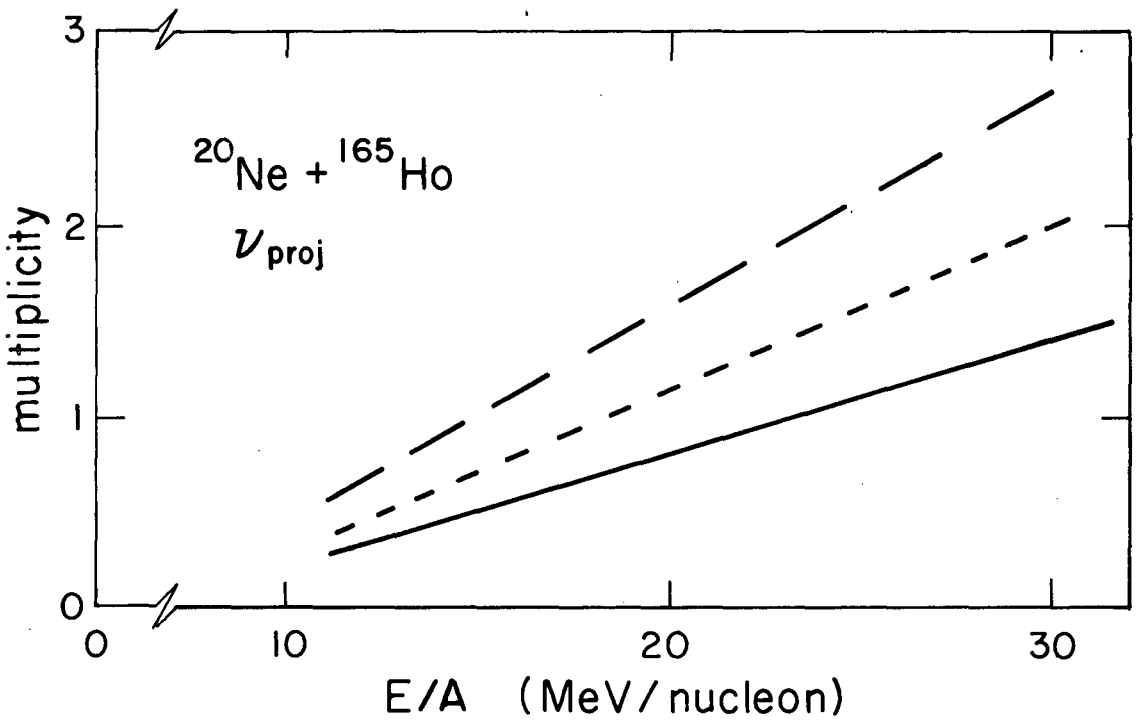

XBL 876-3006

Figure 5.

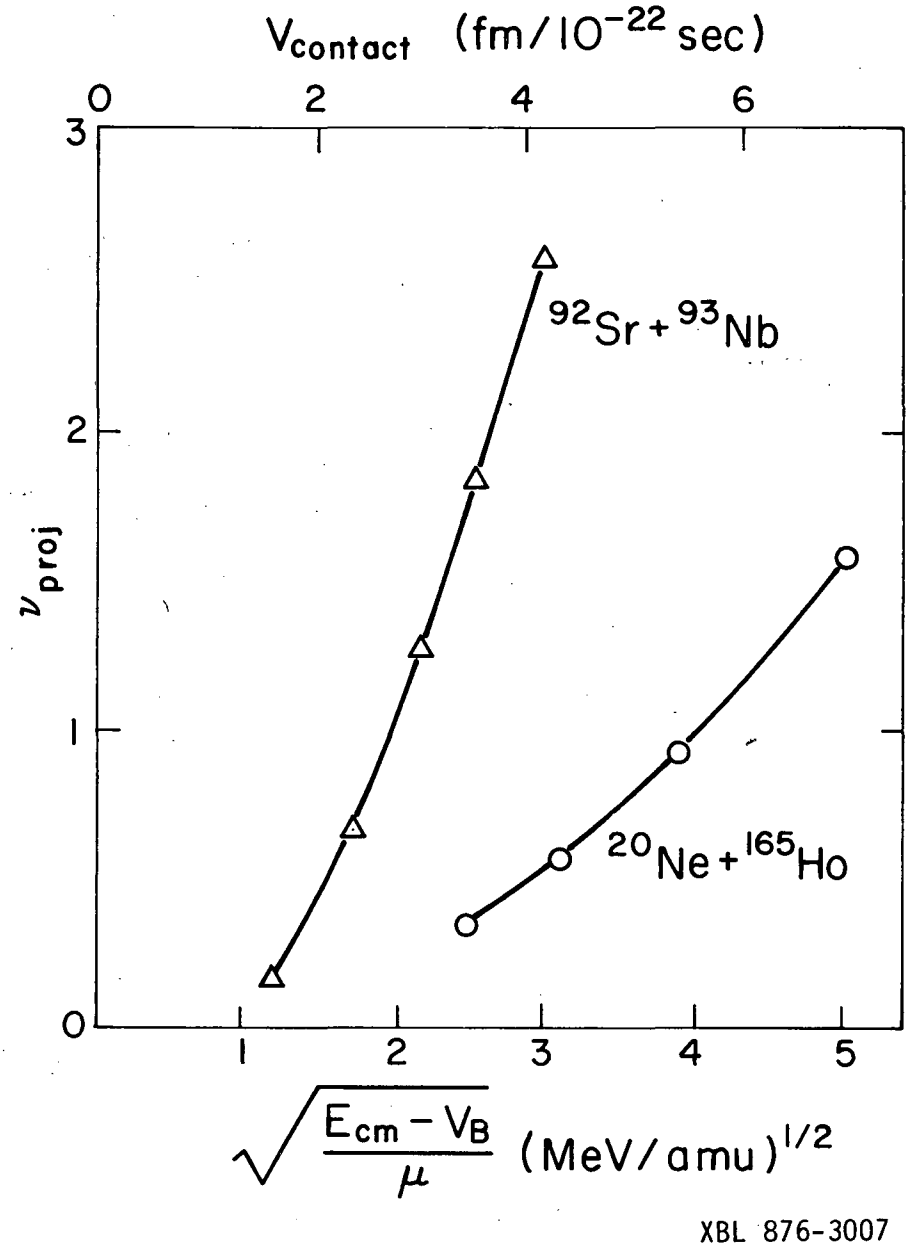
$V_{contact}$ (fm/10^{-22} sec)
0
2
4
6
3
2
1
0
ν_{proj}
$^{92}Sr + ^{93}Nb$
$^{20}Ne + ^{165}Ho$
1
2
3
4
5
$\sqrt{\frac{E_{cm} - V_B}{\mu}}$ (MeV/amu)$^{1/2}$
XBL 876-3007

Figure 6.

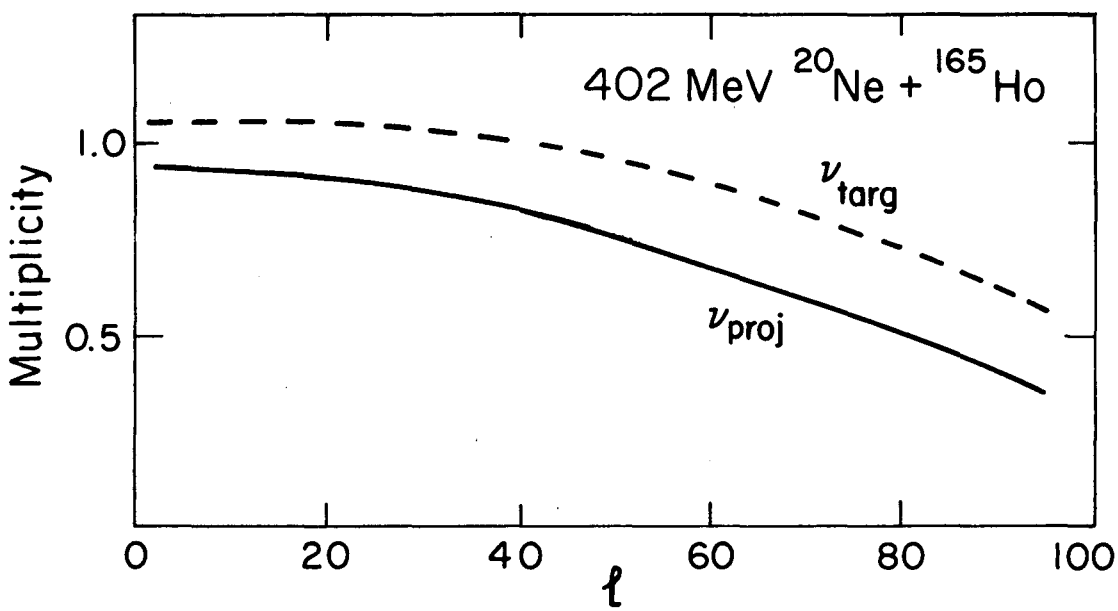

XBL 876-3008

Figure 7.

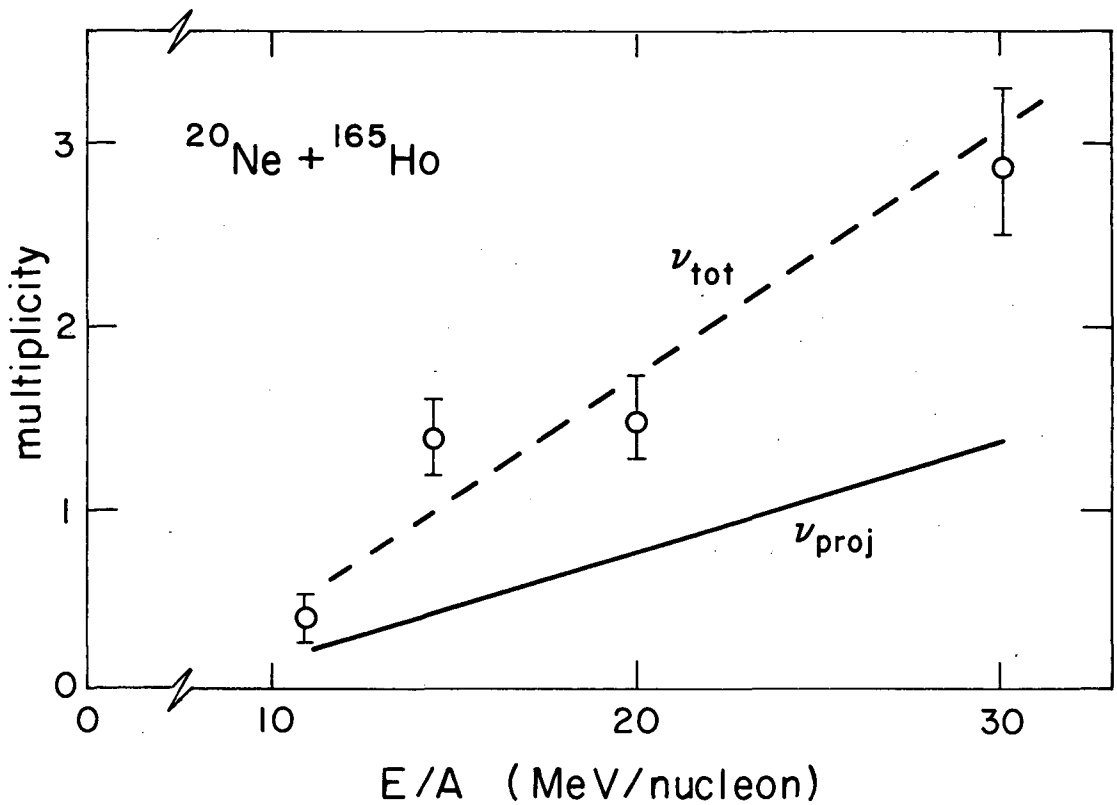

XBL 876-3009

Figure 8.

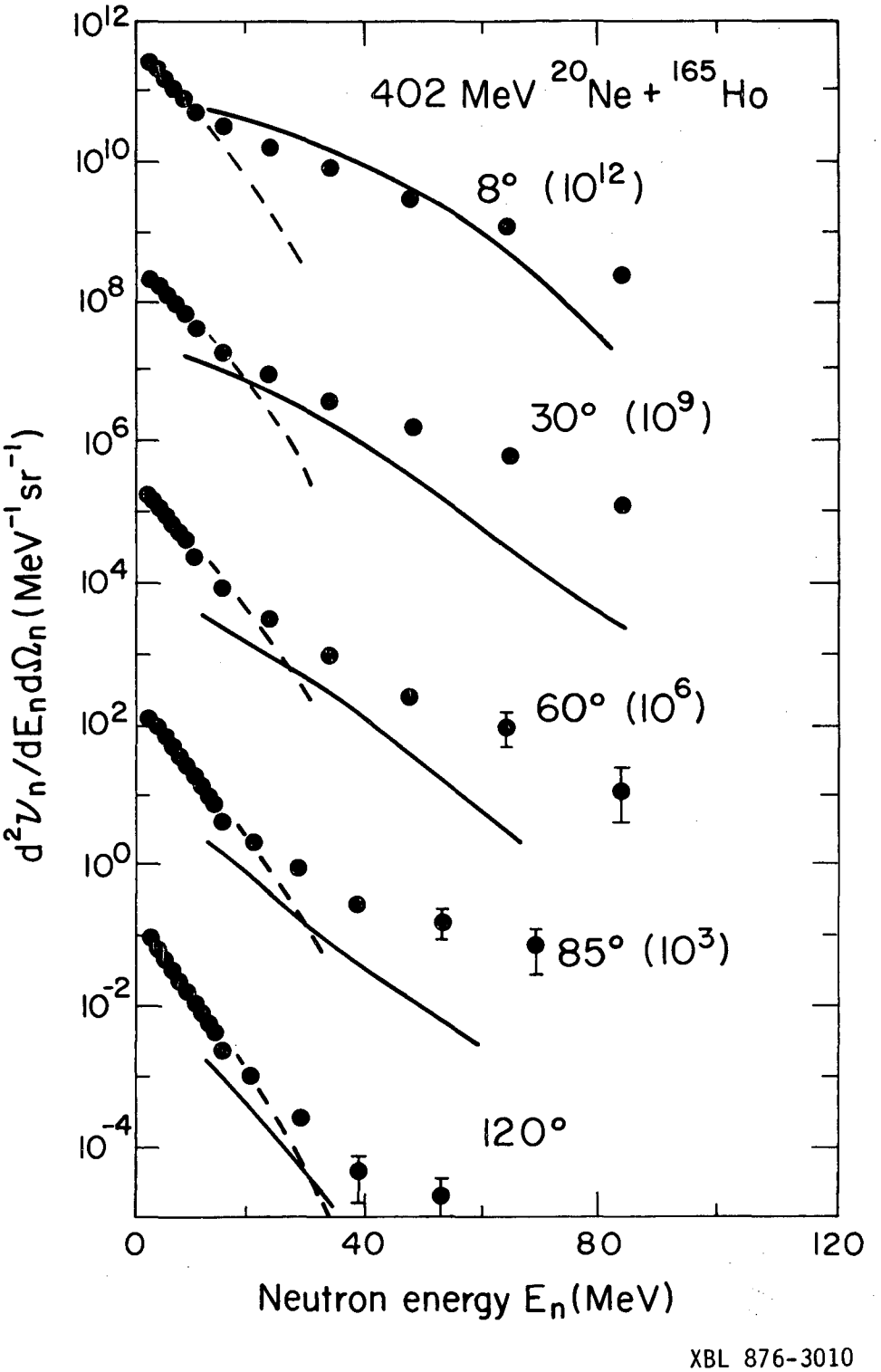
402 MeV ^{20}Ne + ^{165}Ho
8° (10^{12})
30° (10^{9})
60° (10^{6})
85° (10^{3})
120°
$d^2\nu_n/dE_n d\Omega_n$ (MeV^{-1}sr^{-1})
Neutron energy E_n(MeV)
XBL 876-3010

Figure 9.

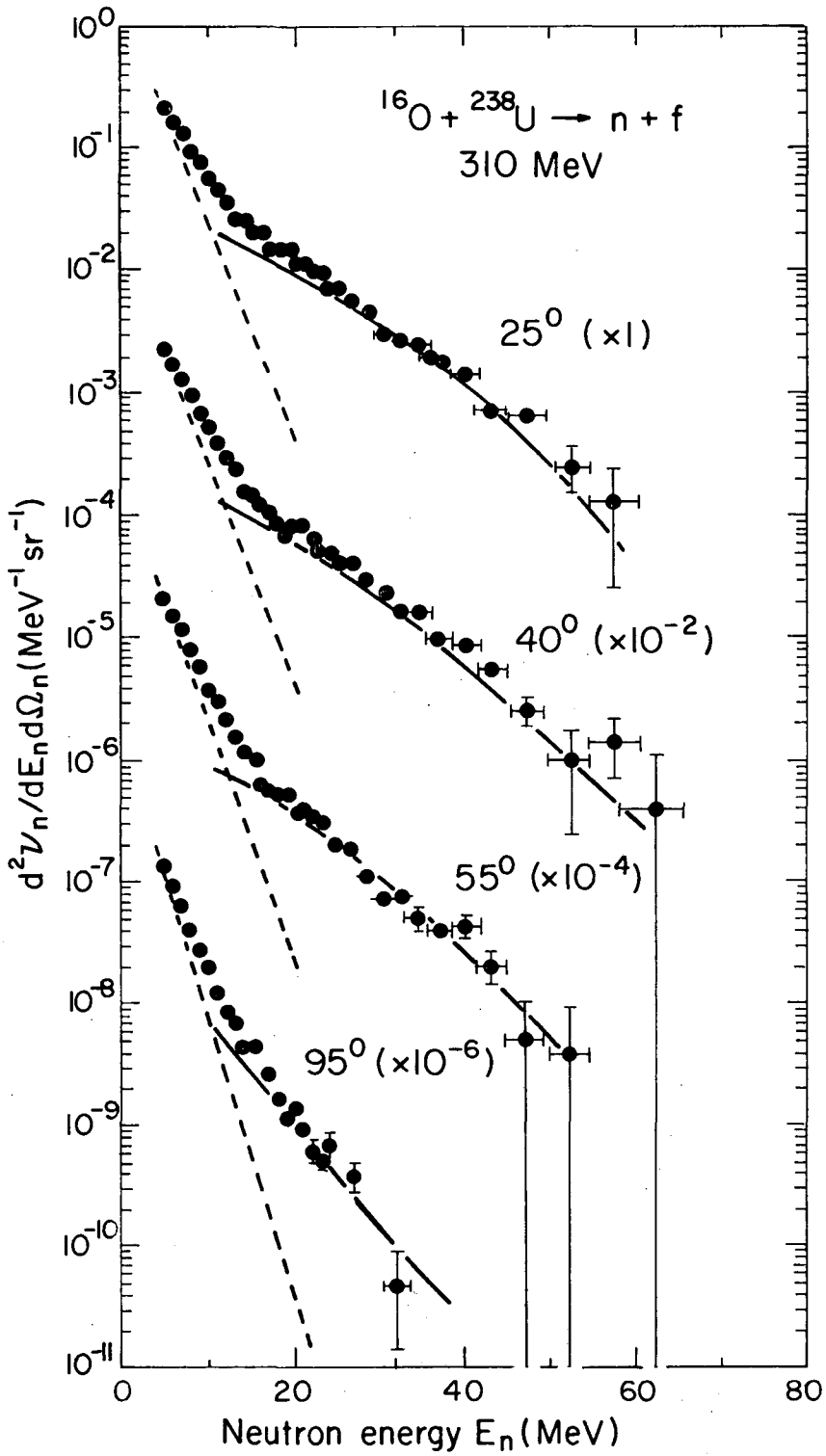
$^{16}O + ^{238}U \rightarrow n + f$
310 MeV
25^0 (×1)
40^0 (×10^{-2})
55^0 (×10^{-4})
95^0 (×10^{-6})
$d^2\nu_n/dE_n d\Omega_n (MeV^{-1} sr^{-1})$
Neutron energy E_n (MeV)
XBL 876-3011

Figure 10.

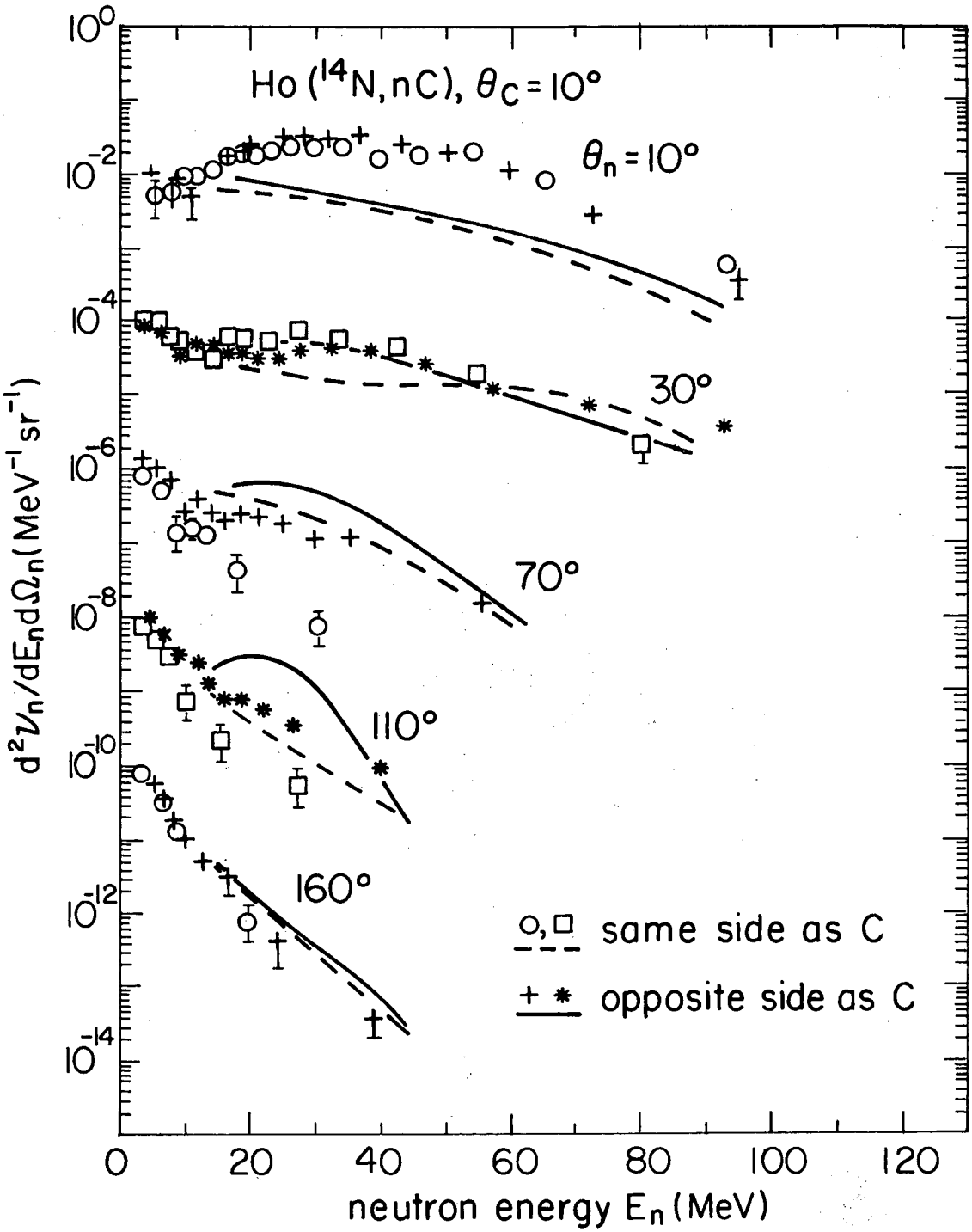

XBL 876-3012

Figure 11.

LAWRENCE BERKELEY LABORATORY
TECHNICAL INFORMATION DEPARTMENT
UNIVERSITY OF CALIFORNIA
BERKELEY, CALIFORNIA 94720